Paper-based Insulator Electrokinetics for Microscale Particle Manipulation and Analysis

Md Nazibul Islam, Satchit Nagpal, Zachary R Gagnon*
Artie McFerrin Department of Chemical Engineering, Texas A&M University, USA. E-mail: zgagnon@tamu.edu

Abstract

Insulator-based electrokinetics (iEK) integrates insulating structures within microchannels to induce local curvature in electric field lines, resulting in regions of high field intensity. This technique has been employed in various applications, such as DNA enrichment, liquid biopsy, biomarker screening, and protein folding analysis, among others. In this paper, we present a new electrokinetic particle manipulation technique using insulating paper fibers to generate high electric field gradients. The technique involves confining nonwoven fiberglass paper channels and copper tape electrodes within thin PDMS sheets fabricated using a low-cost paper-PDMS technique called “Microfluidic pressure in paper” (μPiP). We apply an AC electric field perpendicular to the flow direction to dielectrophoretically trap and separate different polystyrene particles within the paper channels. We further present a 2D computational model of the paper structure and introduce the concept of a 3D “paper unit cell” to analyze the formation of regions with high electric field gradients within the paper structure. This model will be useful for researchers studying paper-based electrochemical sensors, paper-based free-flow electrophoresis and isotachophoresis devices, and lateral flow assays. This new platform enables the development of robust, low-cost, and portable next generation microscale electrokinetic systems for a wide variety of sample purification, quantification and liquid handling applications.

1. Introduction

Insulator-based electrokinetics (iEK) has received significant attention as a tool for developing high-throughput microfluidic devices for biomolecule manipulation. The iEK technique integrates insulating structures within a microchannel, which induce local curvature in the electric field lines, resulting in regions of high field intensity when an electric field is applied to the channel. These regions can be utilized to selectively trap suspending particles, cells, and biomolecules in the surrounding flow field. An essential feature of iEK is its purely physical nature, which eliminates the need for any chemical reaction, making iEK-based devices simpler to fabricate compared to chemical assay-based devices. In addition, iEK can manipulate a broad range of particles, from nanoparticles to macromolecules [1]. Since the biomolecules are not in direct contact with the electrodes, iEK can trap and maintain the viability of sensitive cell lines, such as mammalian cells, making iEK one of the few technologies suitable for developing high-throughput mammalian cell screening devices [2]. Over the years, iEK has been employed in diverse applications, such as liquid biopsy, DNA enrichment, analysis of neural stem cells, biomarker screening, protein folding analysis, and molecular sensing [1–13].

A wide range of insulating structures and curved channels have been employed by various groups to generate a non-homogeneous electric field distribution. One of the earliest reported uses of iEK-based manipulation of biomolecules was in 1989, when Masuda et al. utilized a set of insulating pillar structures to trap two cell species, followed by the application of a pulsed voltage to initiate cellular fusion [14]. In 2000, Cummings and Singh introduced a novel microdevice containing a set of evenly spaced insulating posts etched into a glass microchannel [15]. This insulating post geometry has since become popular in iEK applications, enabling the trapping and separation of micro and nanoparticles, differentiation between dead and live bacteria, and the trapping of proteins and nucleic acid molecules. The Lapizco-Encinas group has made significant contributions to the advancement of microdevices based on pillar structures by optimizing the electrode geometry and studying the effects of suspending media conductivity and pH on particle trapping [3–5,16–23]. Recently, this group has reported an innovative pillar-based iEK technique to separate highly similar micron-sized particles based on surface charge, enabling the separation of cells based on size, genus, or strain [16]. Georg R. Pesch analyzed the effects of post and medium geometries, aspect ratios, and materials on electric polarization, the resulting disturbances, and the possibility of DEP particle trapping [49-50]. The Ros group proposed an approach that utilizes a combination of micron-sized triangular and nano-sized rectangular posts within the same microchannel to create nano-constrictions and reduce the electric potential required for trapping [24]. The Morgan group used insulating pillars to combine deterministic lateral displacement (DLD) with dielectrophoresis (DEP) to continuously separate 100-nm, 500-nm, and 1-μm particles [25,26].

Another technique for creating a non-homogeneous electric field in a microchannel involves fabricating insulating structures within the microchannel wall. The Hayes research group is a pioneer in this approach and has developed iEK devices based on saw-tooth geometric gradients. These devices use microchannel walls with pointed triangular teeth-like patterns as insulating field curvature-inducing structures [27]. The saw-tooth structures gradually increase in size down the channel and create zones of increasing electric field, which have been successfully utilized for selective manipulation of bacterial species, concentration of viruses, trapping of Aβ amyloid fibrils, and separation of human blood cells and biomarkers [6,7,28,29]. The Buie research group has developed a 3D constriction-based iEK technique to discriminate between the strains of pathogenic *Streptococcus mitis* and *Pseudomonas aeruginosa* and has shown that the 3D constrictions require a lower voltage thus reducing Joule heating [30].

In addition to insulating structures, the microchannel geometry itself can be used to generate non-homogenous electric field by fabricating curved channel walls. The Xuan research group has leveraged the electric field distortion formed by the curvature of the channel walls to achieve continuous size-based separation of microparticles [31–33].

Moreover, iEK systems based of insulating microporous membranes and naturally occurring macroscopic porous materials have been reported to manipulate cells and microparticles [34–37].

Herein, we report a new, low-cost and scalable iEK-based particle manipulation technique that leverage the insulating properties of paper fibers to generate zones of high electric field gradients. Recently, we have reported a low-cost, reliable, and scalable paper-PDMS fabrication technique called “Microfluidic pressure in paper” (μPiP) where we utilize a laser to rapidly cut paper fluidic channels at micron-scale resolution [38]. We then confine and chemically seal these paper channels within the PDMS membranes using a combination of corona plasma treatment and benchtop thermal press. We utilize the μPiP to confine nonwoven fiberglass paper channels and copper tape electrodes within thin PDMS sheets. We apply a flow of polarizable microparticles directly within the nonwoven channel and simultaneously apply an AC electric field perpendicular to the flow direction. Using a combination of micro computed tomography (Micro-CT) and finite element analysis, we then present a computational model to demonstrate micro-scale DEP force formation dynamics within nonwoven structure. We further investigate the effect of paper microstructure on DEP force growth dynamics and develop the concept of a "Paper Unit Cell" by employing a micrograph of paper to create a three-dimensional model of a small volume of the paper structure. Similar unit cell models have been used for stochastic modeling of microstructures to study cross-correlation of fiber volume fraction of adjacent mi-crostructures [51]. This 3D model provides a detailed representation of the internal structure of paper and illustrates the process of the formation of regions with high electric field gradients that occur between two individual paper fibers. We further analyze the effect of fiber density within a unit cell on DEP force growth. This model will be a useful tool for researchers studying the properties and behavior of paper in various applications such as lateral flow assays, paper-based electrochemical sensors and, paper-based free-flow electrophoresis and isotachophoresis devices. Motile bacteria move through 3D porous media remains completely unknown [52] and our study attempts to bridges gaps in knowledge of bacterial motility in unconfined electrical charged porous structure. Finally, we demonstrate dielectrophoretic trapping and separation of two different polystyrene particles using fiberglass paper. This new platform offers a cost-effective and scalable alternative to traditional insulator-based electrokinetic fabrication techniques. We believe this will have significant implications for the development of practical applications in a variety of fields, including microfluidics, biosensing, and lab-on-a-chip technologies.

2. Theory

When an electric field is applied across a paper channel, the paper fibers act as insulating structures and generate an electric field gradient. The DEP force acting on a spherical particle moving through the paper structure is dependent on this electric gradient and can be expressed as [39,40]:

$$\boldsymbol{F_{DEP} = 2\pi\varepsilon_o\varepsilon_m r^3 Re[K(\omega)]\nabla|E|^2} \quad (1)$$

Where, ε_o, ε_m, r and $\nabla|E|^2$ are the permittivity of free space, dielectric constant of the media, the radius of the particle and the gradient of the electric field squared respectively and Re[K(ω)] is the real part of Clausius–Mossotti factor (CMF) [39,40]:

$$\mathbf{K}(\boldsymbol{\omega}) = \frac{\boldsymbol{\varepsilon_p^* - \varepsilon_m^*}}{\boldsymbol{\varepsilon_p^* + 2\varepsilon_m^*}} \quad (2)$$

Equation 2, describes the polarizability of a particle (p) in a medium (m) and is based on the complex permittivity ε*, which can be expressed as [40,41]:

$$\boldsymbol{\varepsilon^* = \varepsilon - i\frac{\sigma}{\omega}} \quad (3)$$

Where, ε is the dielectric constant, and σ is the electrical conductivity of the medium and ω is the frequency. The complex K(ω) factor has an imaginary component which is out of phase with the applied electric field and exerts a torque on the particle that can be detected by particle electrorotation [41]. More importantly, the DEP force is dependent on the in phase real part of the K(ω) factor as shown in equation 1.

In addition to the DEP force, a particle flowing through a fluid experiences a drag force. For a pressure driven laminar fluid flow through a micron scale channel, the Navier-Stokes' equation can be simplified, and the drag force can be approximated by the following equation [42–44]:

$$\boldsymbol{F_{HD} = 6\pi\eta r v} \quad (4)$$

Where, η and v are the fluid viscosity and velocity respectively. In order to trap a particle, the DEP force must be equal or stronger than the drag force [43,44]. Therefore, a tapping zone inside the porous structure of paper is formed when:

$$\boldsymbol{F_{DEP} \geq F_{HD}} \quad (5)$$

3. Methods

3.1 Device Fabrication and Micro-CT Analysis

The fabrication workflow for paper based dielectrophoretic trapping device is based on our recently developed fabrication technique called microfluidic pressure in paper (µPiP) [38]. The entire fabrication process, from design to device takes less than 10 minutes to complete. The fabrication begins by first cutting a microfluidic straight channel geometry (4 mm wide, 40 mm long) from a sheet of Craneglas® 230 paper (Neenah Filtration) using a CO_2 laser cutter (LS-2440, Boss Laser). A set of two copper tape electrodes (9 mm wide, 30 mm long, 3M™) are placed on the axial direction of the paper channel with 1 mm gap between them. Each paper channel and copper tape electrodes are then sealed between two thin flexible polydimethylsiloxane (PDMS) sheets (0.5 mm, McMaster-Carr). Fluidic channel inlets/outlets are hole punched on the top PDMS sheet using a 0.75 mm biopsy punch (Ted Pella, Inc.). The two sheets are then oxidized and irreversibly bonded together using oxygen plasma generated with a handheld tesla coil (Electro-Technic Products, Model BD-20AC) and a bench top heat press (Dulytek DW 400). Copper wires are used to connect electrodes to an external voltage generator. The final device assembly is depicted in Figure 1. The paper channels were soaked in 3% w/v BSA (Sigma) in diH2O for twenty minutes and dried prior to experimental use. To investigate the porous structure of the insulating fibers and the resulting distribution of the DEP force, Micro-CT scans of the paper substrate were captured using the SkyScan 1272 bench top micro-CT scan. CTvox software was used to generate 3D images from the scanning results (1.5µm voxel size, 800 ms exposure time) and the resulting micrographs were digitally converted into a 3D structure and used as a computational domain for finite element analysis via a finite element Multiphysics software (COMSOL Inc., Burlington, MA).

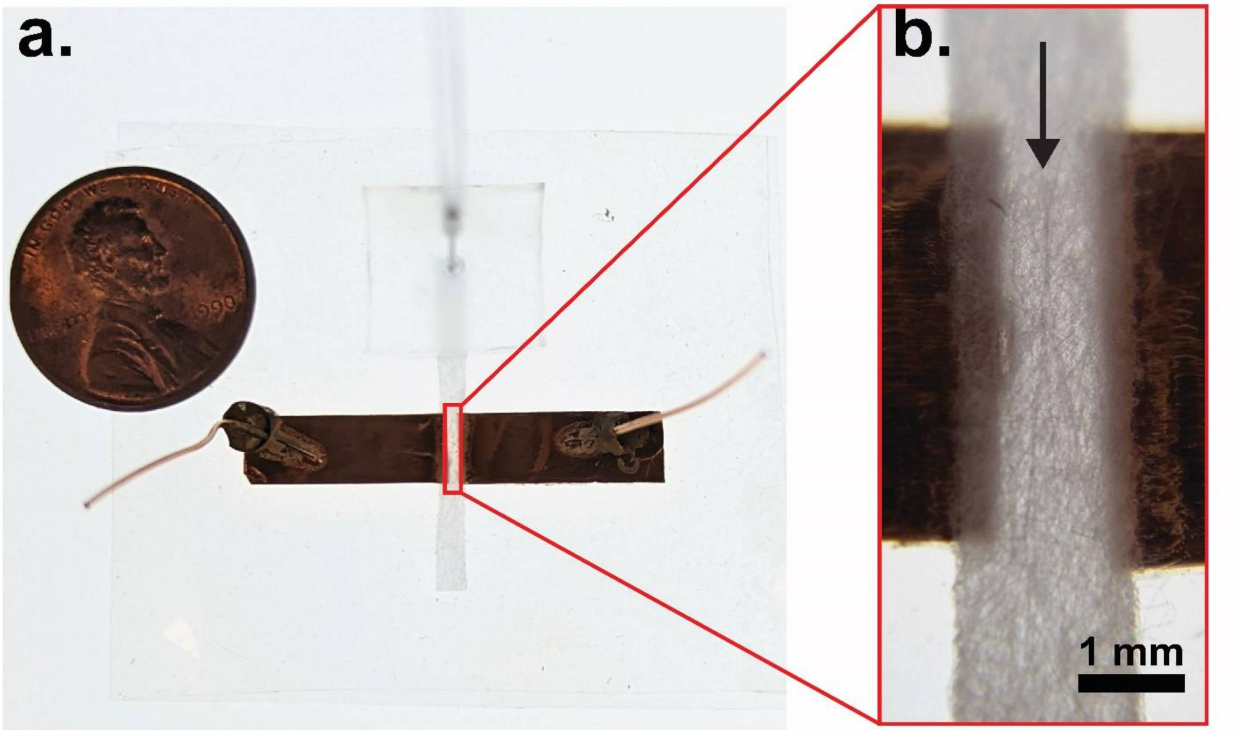

Figure 1: A) Fully assembled µPiP-DEP Device. B) Region of interest for electric field application and DEP force generation

3.2 Experimental Setup and Operation

DEP trapping experiments were performed using fluorescent polystyrene micro-particles with diameters of 1 µm (dragon green) and 4 µm (flash red), obtained from Bangs Laboratories, Inc. The particles were suspended in deionized water and then diluted to a concentration of 8×10^5 1 µm particles and 2.45×10^5 4 µm particles per mL (conductivity: 1 µS/cm, pH: 6.8). To minimize particle agglomeration, 5 wt% Tween 20 was added to the solution.

A 2D quadruple electrode device was fabricated using a previously reported technique [40]. Briefly, chromium and gold were vapor-deposited on a glass cover slide using an e-beam (Lesker PVD 75 Electron Beam Evaporator), and the electrodes were etched on the glass cover slide using a wet-etching technique. A function generator (Rigol DG4102) was used to deliver a 20 V sinusoidal peak-to-peak voltage to the quadruple electrodes. For paper-DEP experiments, the function generator was connected to a 40-dB gain RF amplifier (Mini-Circuits, ZHL-5W-1+) to deliver a 6.2 V sinusoidal peak-to-peak voltage to the copper electrodes. A syringe pump (Chemyx Fusion 100) was used to flow the particle solution at a rate of 4 µL/min through the paper channel. A handheld thermal camera (FLIR TG165) was used to observe any Joule heating effects, and no increase in temperature was observed at the operating voltage range.

4. Results and Discussions

4.1 Finite Element Analysis

This section outlines the finite element analysis method we developed to investigate the trapping mechanism of particles within the porous structure of paper. We first captured a micro-CT scan image of a paper channel using a benchtop CT scanner, which we then converted into a 3D image (Figure 2a). The 3D image revealed that the paper's fiber orientation is anisotropic, with one particular axis having a higher fiber orientation than the others. To generate a maximum gradient and minimum fluidic resistance, we directed the fluid flow towards the fiber direction and applied an electric field across the fiber orientation direction.

Next, we employed a finite element Multiphysics software (COMSOL Inc., Burlington, MA) to explore the formation of electric field gradient zones within paper pores. The model consisted of a 2D representation of the paper porous structure generated from the 3D micro-CT image. This 2D approximation has been previously used to model electric field gradient in iDEP devices based on the assumption that electric potential is relatively consistent across the small depth of the fluidic channel [6,45]. The boundaries of the paper fiber structures were set as insulators, and water was assigned to the bounded domain. One side of the paper structure, parallel to the fiber direction, was defined as ground, and a range of voltage potential (0-10 V) was applied to the other side. The distribution of electric potential was determined using the Laplace equation [45]:

$$\boldsymbol{\nabla^2 \varphi = 0} \quad (6)$$

Where, φ is the electric potential and the electric field was determined by [46,47]:

$$\mathbf{E} = -\boldsymbol{\nabla\varphi} \quad (7)$$

Figure 2b and c represents the results for the gradient of the electric field squared ($\nabla|\mathrm{E}|^2$) for the paper structure. The figures demonstrate that paper structures produce regions of high electric field gradient, similar to those of traditional iDEP devices, which can be used to trap, isolate, and concentrate particles from a suspending medium.

One key observation from the finite element analysis result is that the trapping zones formed within paper structures are more heterogeneous in nature compared to traditional iDEP devices. Trapping zones are defined as specific locations within the paper structure with a high DEP force that can trap a moving particle. To better understand the DEP force growth dynamics between different trapping zones, the increase in DEP force expressed as $\nabla|E|^2$ with the increase in applied voltage was measured and plotted at two different trapping zones using the COMSOL model, as shown in Figures 2c and 2d. Figure 2d demonstrates that there is almost a 10-fold difference in DEP force between the two different trapping zones. This heterogeneity in the electric field gradient produced in paper is due to the fact that paper fibers consist of a wide variety of overlapping structures, ranging from parallel and perpendicular aligned fibers that form porous flow regions to converging/diverging sharp and rounded fiber ends that occur at the entrance and exits to these flow regions. Previous research has reported that insulating structures with a sharp end, where the radius of curvature (ROC) changes rapidly, constrict the electric field and produce a larger electric field gradient compared to rounded ends, where the ROC change is more gradual [18,47]. In addition, the distance between two insulating structures varies from one trapping zone to another which also influences the DEP force growth.

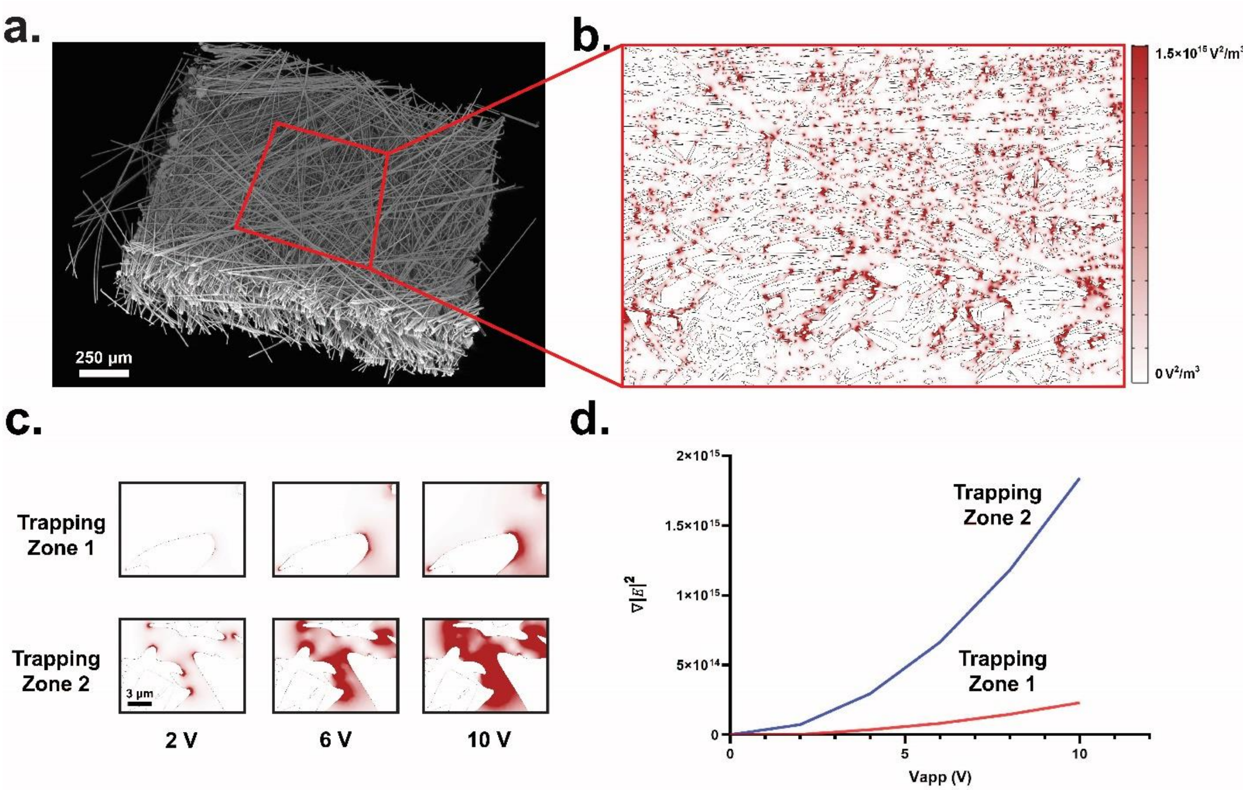

Figure 2: A) Micro-CT scan of a paper-based DEP device. B) Electric field gradient distribution inside porous paper structure. C) Two different trapping zones within paper channel and pore-scale DEP force generation for different applied voltages. D) DEP force growth curves for the two trapping zones.

4.2 Unit-Cell Analysis

While a 2D slice gives us an initial understanding of the paper structure, a 3D model provides a much more comprehensive view of its internal and external features, allowing for a more in-depth comprehension of DEP force growth. Therefore, we have developed a 3D unit cell model that can accurately represent paper structure. Figure 3a illustrates the microscopic arrangement of glass-fiber paper, where each paper fiber is characterized by a cylindrical shape with a diameter of 5 microns. Based on this knowledge, we have constructed a 3D unit cell for paper, comprising three randomly dispersed cylinders, each with a 5-micron diameter as demonstrated in Figure 3b. Subsequently, we utilized the finite element analysis method to apply an external electric field and measure the DEP force between paper fibers. Figures 3c and d represent the isometric and front views of the paper unit cell subjected to an external electric field. As can be seen from these figures, the region of high electric field gradient, i.e., DEP force, is formed between the adjacent paper fibers. This is because as the electric field lines pass through this structure, they must converge/diverge the most at these regions, thus creating regions of high field gradient. More interestingly, the formation of trapping zones within paper structures appears to be similar to those formed in a traditional pillar-based iDEP device (Figure 3e). In both cases, the trapping zones are formed between two adjacent insulating structures. Therefore, particle trapping in paper occurs in a manner like that in an insulating pillar-based device.

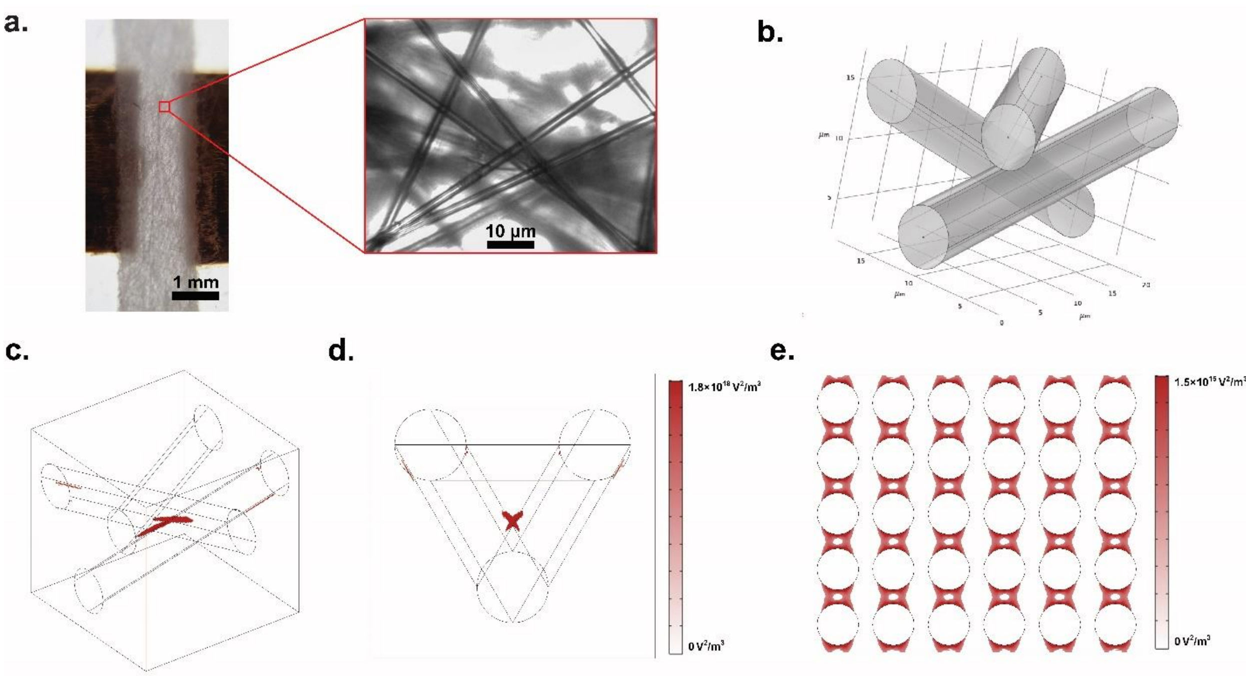

Figure 3: Investigation of porous structure of paper. A) Microscopic image of glass-fiber paper. B) 3D model of a unit paper cell. C) Isometric view of induced DEP force generated within the unit cell. D) Front view of the unit cell with induced DEP force. E) DEP force distribution in a traditional iDEP device.

Based on the findings from unit cell analysis, we posit those physical properties such as fiber diameter, density, and structure play an important role in DEP force growth within a paper channel. In the case of the same paper type, DEP force growth will differ based on the distance between two insulating fibers, i.e., fiber density within a unit cell. To test this hypothesis, we constructed unit cells that have different fiber densities (number of fibers within a fixed volume) as shown in Figure 4a. We then calculated the average DEP force within the unit cell. This result was plotted in Figure 4b, which illustrates that the DEP force growth will increase with an increase in fiber density. However, this increase is not linear and approaches a plateau as we increase fiber density. From this analysis, we concluded that the heterogeneity we observed in our 2D analysis was due to the heterogeneity in fiber density within the paper channel. In the future, we plan to develop a physics-based model that considers different paper fiber features to generate the electric field distribution and velocity profile for a particular structure.

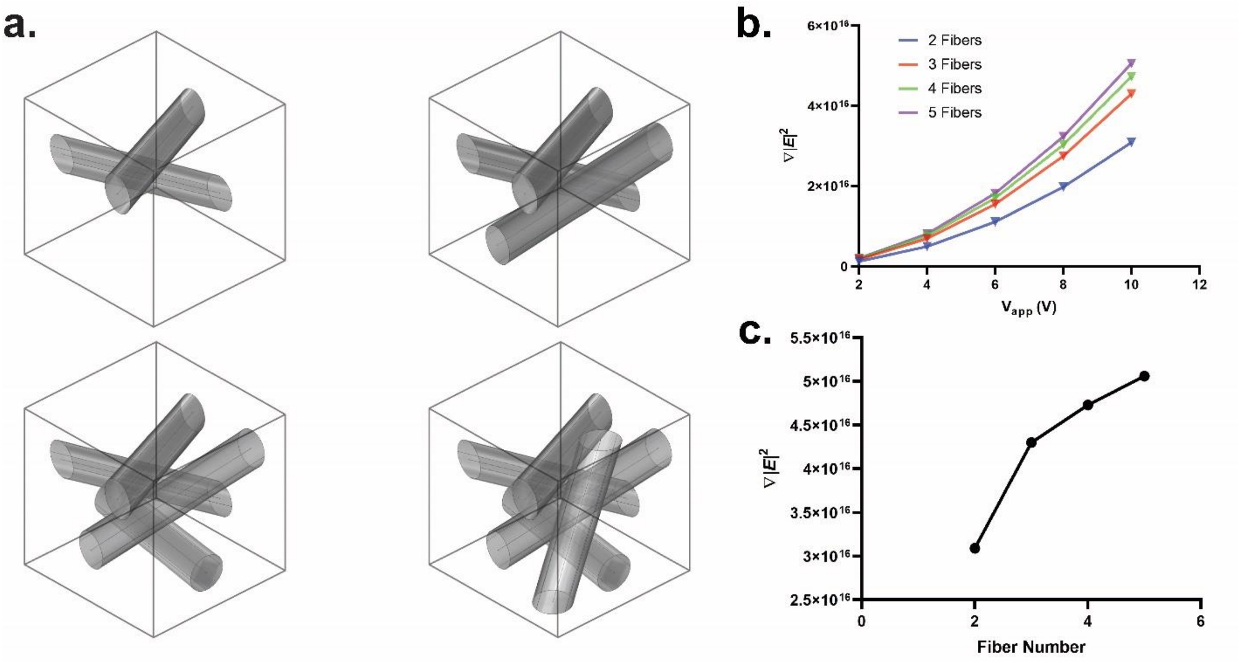

Figure 4: Investigation of fiber density on DEP force dynamics. A) Unit cells with 2,3,4, and 5 cylindrical fibers. B) DEP force growth dynamics for unit cells with different fiber density. C) DEP for generated within unit cells with different fiber densities for 10V applied electric field

4.3 Separation of PS Particles Using Paper-DEP

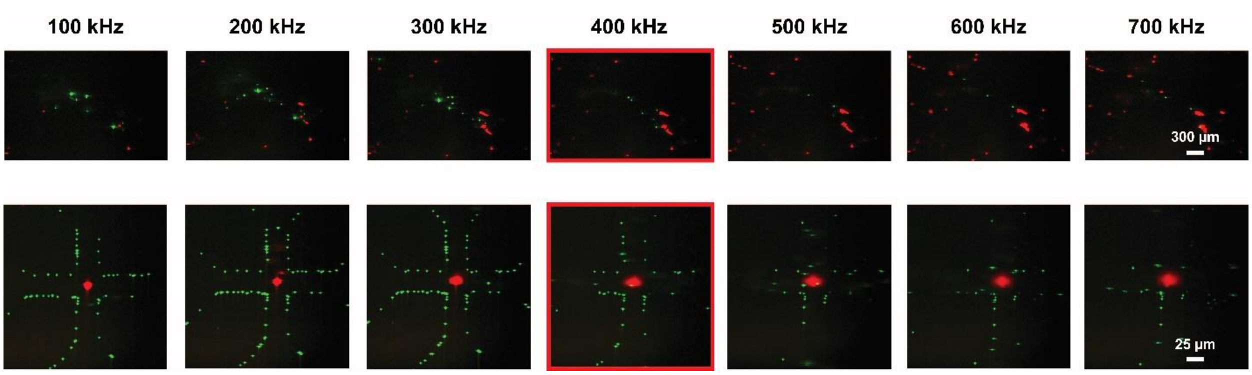

Figure 5: Comparison of PS particle assembly using AC DEP between paper DEP and traditional 2D electrode-based DEP devices. The particle assembly shows a similar trend between paper and 2D electrode DEP devices. The smaller green particles exhibit positive DEP at low frequency and get released from both the planner electrodes and paper pores after 400 kHz. The larger red particles exhibit negative DEP throughout the applied frequency range.

We now present an experimental demonstration of paper-based dielectrophoretic particle trapping and separation and compare it to a traditional 2D thin-film electrode array with quadrupole structures (Figure 5). We used two different fluorescent PS micro-particles with diameters of 1 µm (dragon green) and 4 µm (flash red) suspended in deionized (DI) water medium. For paper DEP, PS particles were flowed through paper at a constant flowrate of 4 µL/min and for the thin-film device, 5 µL of particle suspension was pipetted on the electrode array. A function generator was used to deliver 20 V sinusoidal peak-to-peak voltage to the alternate quadrupole electrodes and the other two electrodes were grounded. For paper DEP, the function generator was connected to a 40-dB gain RF amplifier to deliver 6.2 V sinusoidal peak-to-peak voltage to the copper electrode. As with RC circuits, DEP systems have a fixed cutoff frequency (determined by the thickness and composition of the insulating membrane), preventing testing DEP on particles over a wide frequency range [48]. The DEP behavior of the PS particles was experimentally determined using the quadruple electrodes for a range of AC frequencies (100 kHz to 1 MHz). As shown in Figure 5, the 4-micron red particles experience negative DEP within this frequency range. For the 1-micron green particles, the particles experience positive DEP at low frequencies and reach the crossover frequency (COF) at around 400 kHz, experiencing a weak negative DEP force afterward. When we compare this finding with our paper-DEP device, we observe that at low frequencies, the green particles are getting trapped in the paper pores, and as we approach COF, the particles get released from their trapping zones, indicating that the magnitude of the drag force is higher than the DEP force at these frequencies. In the case of the red particles, we observe that more and more particles are getting trapped within the paper pores as we increase the frequency. This is because the particles are experiencing a high negative DEP force within the applied frequency range, and because of the constant flow rate, there is a constant flux of particles entering the trapping zone. Therefore, with time, more and more particles get trapped. Hence, paper-DEP can be used to selectively trap, and separate particles based on their COF.

Conclusions

In conclusion, we have demonstrated a new DEP mechanism that leverages the insulating properties of paper fibers to generate regions of high electric field gradient and DEP force within the paper structure that acts as trapping zones for microparticles. We have utilized finite element analysis to develop a 2D model of a paper channel and presented the concept of a 3D "paper unit cell" to investigate the effects of fiber structure on pore-scale trapping zones. Our results indicate that the density of fibers plays a crucial role in the growth dynamics of DEP force, leading to varying DEP force for different trapping zones under a given applied electric potential. This heterogeneity can be mitigated by designing paper substrates with homogenous fiber density. Additionally, our simulation results indicate that the location of trapping zones formed within paper unit cell are similar to those generated in traditional pillar-based devices. Additionally, we have successfully demonstrated particle trapping and COF-based separation using AC DEP and compared paper-based DEP with a 2D electrode-based DEP device. Our findings highlight the potential of our low-cost and scalable iEK-based particle manipulation technique to revolutionize the field of microfluidics by making it more accessible to researchers and industries alike.

Acknowledgement

The PI gratefully acknowledges support from a NASA Early Career Faculty award (80NSSC19K1401) and NSF I Corps award (2112224).

Reference

[1] B.H. Lapizco-Encinas, The latest advances on nonlinear insulator-based electrokinetic microsystems under direct current and low-frequency alternating current fields: a review, (n.d.). https://doi.org/10.1007/s00216-021-03687-9/Published.

[2] P. Benhal, D. Quashie, Y. Kim, J. Ali, Insulator based dielectrophoresis: Micro, nano, and molecular scale biological applications, Sensors (Switzerland). 20 (2020) 1–24. https://doi.org/10.3390/s20185095.

[3] A. Vaghef-Koodehi, O.D. Ernst, B.H. Lapizco-Encinas, Separation of Cells and Microparticles in Insulator-Based Electrokinetic Systems, Anal Chem. 95 (2023) 1409–1418. https://doi.org/10.1021/acs.analchem.2c04366.

[4] H. Moncada-Hernández, B.H. Lapizco-Encinas, Simultaneous concentration and separation of microorganisms: Insulator-based dielectrophoretic approach, Anal Bioanal Chem. 396 (2010) 1805–1816. https://doi.org/10.1007/s00216-009-3422-4.

[5] B.H. Lapizco-Encinas, R. V. Davalos, B.A. Simmons, E.B. Cummings, Y. Fintschenko, An insulator-based (electrodeless) dielectrophoretic concentrator for microbes in water, J Microbiol Methods. 62 (2005) 317–326. https://doi.org/10.1016/j.mimet.2005.04.027.

[6] J. Ding, R.M. Lawrence, P. V. Jones, B.G. Hogue, M.A. Hayes, Concentration of Sindbis virus with optimized gradient insulator-based dielectrophoresis, Analyst. 141 (2016) 1997–2008. https://doi.org/10.1039/c5an02430g.

[7] J. Ding, C. Woolley, M.A. Hayes, Biofluid pretreatment using gradient insulator-based dielectrophoresis: separating cells from biomarkers, Anal Bioanal Chem. 409 (2017) 6405–6414. https://doi.org/10.1007/s00216-017-0582-5.

[8] P. V Jones, G.L. Salmon, A. Ros, Continuous Separation of DNA Molecules by Size Using Insulator-Based Dielectrophoresis, Anal. Chem. 89 (2017) 21. https://doi.org/10.1021/acs.analchem.6b03369.

[9] B.H. Lapizco-Encinas, S. Ozuna-Chacón, M. Rito-Palomares, A. Malekanfard, S. Beladi-Behbahani, T.R. Tzeng, H. Zhao, X. Xuan, M. Viefhues, R. Eichhorn, B.H. Lapizco-Encinas, O. Eisen, S. Rang, A. Talvari, Protein manipulation with insulator-based dielectrophoresis and direct current electric fields, Electrophoresis. 93 (2019) 1483–1506. https://doi.org/10.1016/j.chroma.2008.05.077.

[10] S.K. Srivastava, A. Artemiou, A.R. Minerick, Direct current insulator-based dielectrophoretic characterization of erythrocytes: ABO-Rh human blood typing, Electrophoresis. (2011) 2530–2540. https://doi.org/10.1002/elps.201100089.

[11] B.H. Lapizco-Encinas, B.A. Simmons, E.B. Cummings, Y. Fintschenko, Insulator-based dielectrophoresis for the selective concentration and separation of live bacteria in water, Electrophoresis. 25 (2004) 1695–1704. https://doi.org/10.1002/elps.200405899.

[12] A. Abdollahi, H. Shokouhmand, Electrokinetic separation of cfDNA in insulator-based dielectrophoresis systems: a linear model of cfDNA and investigation of effective parameters, Journal of Physics Condensed Matter. 34 (2022). https://doi.org/10.1088/1361-648X/ac6476.

[13] G.J. Mcgraw, R. V Davalos, J.D. Brazzle, J. Hachman, M. Hunter, G.J. Fiechtner, E.B. Cummings, Y. Fintschenko, B.A. Simmons, monitoring of water-borne pathogens Polymeric Insulator-based Dielectrophoresis (iDEP) for the Monitoring of Water-borne Pathogens, (2004).

[14] S. Masuda, M. Washizu, T. Nanba, Novel Method Of Cell Fusion In Field Constriction Area In Fluid Integrated Circuit, IEEE Trans Ind Appl. 25 (1989) 732–737. https://doi.org/10.1109/28.31255.

[15] E.B. Cummings, A.K. Singh, Dielectrophoretic trapping without embedded electrodes, Microfluidic Devices and Systems III. 4177 (2000) 151–160. https://doi.org/10.1117/12.395653.

[16] A. Vaghef-Koodehi, C. Dillis, B.H. Lapizco-Encinas, High-Resolution Charge-Based Electrokinetic Separation of Almost Identical Microparticles, Anal Chem. 94 (2022) 6451–6456. https://doi.org/10.1021/acs.analchem.2c00355.

[17] N. Hill, A.C. De Peña, A. Miller, B.H. Lapizco-Encinas, On the potential of microscale electrokinetic cascade devices, Electrophoresis. 42 (2021) 2474–2482. https://doi.org/10.1002/elps.202100069.

[18] A. LaLonde, A. Gencoglu, M.F. Romero-Creel, K.S. Koppula, B.H. Lapizco-Encinas, Effect of insulating posts geometry on particle manipulation in insulator based dielectrophoretic devices, J Chromatogr A. 1344 (2014) 99–108. https://doi.org/10.1016/j.chroma.2014.03.083.

[19] O.D. Ernst, A. Vaghef-Koodehi, C. Dillis, A. Lomeli-Martin, B.H. Lapizco-Encinas, Dependence of Nonlinear Electrophoresis on Particle Size and Electrical Charge, Anal Chem. (2022). https://doi.org/10.1021/acs.analchem.2c05595.

[20] H. Moncada-Hernandez, J.L. Baylon-Cardiel, V.H. Pérez-González, B.H. Lapizco-Encinas, Insulator-based dielectrophoresis of microorganisms: Theoretical and experimental results, Electrophoresis. 32 (2011) 2502–2511. https://doi.org/10.1002/elps.201100168.

[21] J.L. Baylon-Cardiel, N.M. Jesús-Pérez, A. V. Chávez-Santoscoy, B.H. Lapizco-Encinas, Controlled microparticle manipulation employing low frequency alternating electric fields in an array of insulators, Lab Chip. 10 (2010) 3235–3242. https://doi.org/10.1039/c0lc00097c.

[22] A. Lomeli-Martin, O.D. Ernst, B. Cardenas-Benitez, R. Cobos, A.S. Khair, B.H. Lapizco-Encinas, Characterization of the Nonlinear Electrophoretic Behavior of Colloidal Particles in a Microfluidic Channel, Anal Chem. (2023). https://doi.org/10.1021/acs.analchem.3c00782.

[23] B. Cardenas-Benitez, B. Jind, R.C. Gallo-Villanueva, S.O. Martinez-Chapa, B.H. Lapizco-Encinas, V.H. Perez-Gonzalez, Direct Current Electrokinetic Particle Trapping in Insulator-Based Microfluidics: Theory and Experiments, Anal Chem. 92 (2020) 12871–12879. https://doi.org/10.1021/acs.analchem.0c01303.

[24] A. Nakano, F. Camacho-Alanis, A. Ros, Insulator-based dielectrophoresis with β-galactosidase in nanostructured devices, Analyst. 140 (2015) 860–868. https://doi.org/10.1039/c4an01503g.

[25] V. Calero, P. Garcia-Sanchez, C. Honrado, A. Ramos, H. Morgan, AC electrokinetic biased deterministic lateral displacement for tunable particle separation, Lab Chip. 19 (2019) 1386–1396. https://doi.org/10.1039/c8lc01416g.

[26] V. Calero, P. García-Sánchez, A. Ramos, H. Morgan, Electrokinetic biased deterministic lateral displacement: scaling analysis and simulations, J Chromatogr A. 1623 (2020) 461151. https://doi.org/10.1016/j.chroma.2020.461151.

[27] M.D. Pysher, M.A. Hayes, Electrophoretic and dielectrophoretic field gradient technique for separating bioparticles, Anal Chem. 79 (2007) 4552–4557. https://doi.org/10.1021/ac070534j.

[28] P. V Jones, S. Huey, P. Davis, R. Mclemore, A. Mclaren, M.A. Hayes, Biophysical separation of Staphylococcus epidermidis strains based on antibiotic resistance, Analyst. 140 (2015) 5152. https://doi.org/10.1039/c5an00906e.

[29] S.J.R. Staton, P. V Jones, G. Ku, S.D. Gilman, I. Kheterpal, M.A. Hayes, Manipulation and capture of Ab amyloid fibrils and monomers by DC insulator gradient dielectrophoresis (DC-iGDEP) †, (n.d.). https://doi.org/10.1039/c2an35138b.

[30] W.A. Braff, D. Willner, P. Hugenholtz, K. Rabaey, C.R. Buie, Dielectrophoresis-Based Discrimination of Bacteria at the Strain Level Based on Their Surface Properties, PLoS One. 8 (2013). https://doi.org/10.1371/journal.pone.0076751.

[31] H. Harrison, X. Lu, S. Patel, C. Thomas, A. Todd, M. Johnson, Y. Raval, T.R. Tzeng, Y. Song, J. Wang, D. Li, X. Xuan, C. Church, J. Zhu, G. Huang, T.R. Tzeng, X. Xuan, G. Hu, X. Xuan, Electrokinetic particle entry into microchannels, Analyst. 140 (2010) 2869–2875. https://doi.org/10.1063/1.3496358.

[32] J. Bentor, A. Malekanfard, M.K. Raihan, S. Wu, X. Pan, Y. Song, X. Xuan, Insulator-based dielectrophoretic focusing and trapping of particles in non-Newtonian fluids, Electrophoresis. 42 (2021) 2154–2161. https://doi.org/10.1002/elps.202100005.

[33] S. Patel, D. Showers, P. Vedantam, T.R. Tzeng, S. Qian, X. Xuan, Microfluidic separation of live and dead yeast cells using reservoir-based dielectrophoresis, Biomicrofluidics. 6 (2012). https://doi.org/10.1063/1.4732800.

[34] M. Lorenz, D. Malangré, F. Du, M. Baune, J. Thöming, G.R. Pesch, High-throughput dielectrophoretic filtration of sub-micron and micro particles in macroscopic porous materials, Anal Bioanal Chem. 412 (2020) 3903–3914. https://doi.org/10.1007/s00216-020-02557-0.

[35] G.R. Pesch, F. Du, U. Schwientek, C. Gehrmeyer, A. Maurer, J. Thöming, M. Baune, Recovery of submicron particles using high-throughput dielectrophoretically switchable filtration, Sep Purif Technol. 132 (2014) 728–735. https://doi.org/10.1016/j.seppur.2014.06.028.

[36] G.R. Pesch, M. Lorenz, S. Sachdev, S. Salameh, F. Du, M. Baune, P.E. Boukany, J. Thöming, Bridging the scales in high-throughput dielectrophoretic (bio-) particle separation in porous media OPEN, (n.d.). https://doi.org/10.1038/s41598-018-28735-w.

[37] Y.K. Cho, S. Kim, K. Lee, C. Park, J.G. Lee, C. Ko, Bacteria concentration using a membrane type insulator-based dielectrophoresis in a plastic chip, Electrophoresis. 30 (2009) 3153–3159. https://doi.org/10.1002/elps.200900179.

[38] M.N. Islam, J.W. Yost, Z.R. Gagnon, Microfluidic pressure in paper (μPiP): Rapid prototyping and low-cost liquid handling for on-chip diagnostics, Analyst. 147 (2022). https://doi.org/10.1039/d1an01676h.

[39] R. Pethig, Dielectrophoresis: Status of the theory, technology, and applications, Biomicrofluidics. 4 (2010) 1–35. https://doi.org/10.1063/1.3456626.

[40] E. Lavi, F. Crivellari, Z. Gagnon, Dielectrophoretic detection of electrical property changes of stored human red blood cells _ Enhanced Reader, Electrophoresis. (2022).

[41] A.R. Minerick, DC Dielectrophoresis in Lab-on-a-Chip Devices., In: Li D. (Eds) Encyclopedia of Microfluidics and Nanofluidics. Springer, Boston, MA. (2008). https://doi.org/10.1007/978-0-387-48998-8_294.

[42] N. Piacentini, G. Mernier, R. Tornay, P. Renaud, Separation of platelets from other blood cells in continuous-flow by dielectrophoresis field-flow-fractionation, Biomicrofluidics. 5 (2011). https://doi.org/10.1063/1.3640045.

[43] M. Li, S. Li, W. Cao, W. Li, W. Wen, G. Alici, Improved concentration and separation of particles in a 3D dielectrophoretic chip integrating focusing, aligning and trapping, (n.d.). https://doi.org/10.1007/s10404-012-1071-y.

[44] J. Cao, P. Cheng, F. Hong, A numerical analysis of forces imposed on particles in conventional dielectrophoresis in microchannels with interdigitated electrodes, J Electrostat. 66 (2008) 620–626. https://doi.org/10.1016/j.elstat.2008.09.003.

[45] C. v. Crowther, M.A. Hayes, Refinement of insulator-based dielectrophoresis, Analyst. 142 (2017) 1608–1618. https://doi.org/10.1039/c6an02509a.

[46] D. Chen, H. Du, A microfluidic device for rapid concentration of particles in continuous flow by DC dielectrophoresis, (n.d.). https://doi.org/10.1007/s10404-009-0545-z.

[47] C. V Crowther, M.A. Hayes, Refinement of insulator-based dielectrophoresis, 142 (2017) 1608. https://doi.org/10.1039/c6an02509a.

[48] Perez-Gonzalez, V.H. (2021), Particle trapping in electrically driven insulator-based microfluidics: Dielectrophoresis and induced-charge electrokinetics. ELECTROPHORESIS, 42: 2445-2464. https://doi.org/10.1002/elps.202100123

[49] Pesch, G.R., Kiewidt, L., Du, F., Baune, M. and Thöming*, J. (2016), Electrodeless dielectrophoresis: Impact of geometry and material on obstacle polarization. ELECTROPHORESIS, 37: 291-301. https://doi.org/10.1002/elps.201500313

[50] G. R. Pesch, F. Du, M. Baune, and J. Töming (2017). Influence of geometry and material of insulating posts on particle trapping using positive dielectrophoresis. Journal of Chromatography A 1483, 127–137

[51] Sanei, Seyed Hamid Reza & Fertig III, Ray. (2015). Uncorrelated volume element for stochastic modeling of microstructures based on local fiber volume fraction variation. Composites Science and Technology. 117. 191-198. 10.1016/j.compscitech.2015.06.010.

[52] Bhattacharjee, T., Datta, S.S. Bacterial hopping and trapping in porous media. *Nat Commun* **10**, 2075 (2019). https://doi.org/10.1038/s41467-019-10115-1